Title

Are we conscious at all times?
Neural evidence for a two-stage model of visual processing

Maëlan Q. Menétrey[1,2,3], Michael H. Herzog[1], & David Pascucci[1,2,3]

[1]Laboratory of Psychophysics, Brain Mind Institute, École Polytechnique Fédérale de Lausanne (EPFL), Lausanne, Switzerland

[2]Psychophysics and Neural Dynamics Lab, Department of Radiology, Lausanne University Hospital (CHUV) and University of Lausanne (UNIL), Lausanne, Switzerland

[3]The Sense Innovation and Research Center, Lausanne, Switzerland

Keywords: conscious perception, unconscious processing, neural correlates, EEG decoding

Corresponding author: maelan.menetrey@gmail.com

Number of pages: 39

Number of figures: 6; of supplementary figure: 3

Number of words for abstract: 177; for introduction: 749; for discussion: 1697

Funding: This work was supported by the Swiss National Science Foundation (grant number 325130_204898; grant numbers PZ00P1_179988 and PZ00P1_179988/2; and grant number TMSGI1_218247).

Abstract

Postdictive effects, where later events influence the perception of earlier ones, suggest that conscious perception is not a continuous stream but occurs at discrete moments in time, preceded by extended periods of unconscious processing. This is evident in the Sequential Metacontrast Paradigm (SQM), where a stream of lines and vernier offsets is unconsciously integrated over several hundred milliseconds before a conscious percept emerges. Regardless of whether one or multiple verniers are shown, only a single offset is perceived. Postdictive phenomena offer a unique opportunity to study the neural correlates of unconscious and conscious stages of perception because unconscious and conscious processing are well separated in time. Here, using EEG recordings during the SQM, we identified two distinct stages of neural activity. Early occipital EEG activity patterns (~200 ms after the initial vernier presentation) capture unconscious processing, while later centro-parietal EEG patterns (~400-600 ms after the onset of the stimulus stream) are associated with conscious perception, aligning with behavioral results. We propose that the transition between these distinct neural topographies reflects the discrete moments when conscious perception emerges.

Introduction

Consciousness feels like a continuous stream—we see the world at each moment of time. However, several visual phenomena challenge this idea. For instance, in a classic apparent motion phenomenon, two dots of different colors are flashed at separate locations with a brief delay (Kolers & Von Grünau, 1976). Rather than perceiving two distinct flashes one after the other, we perceive a single moving dot that changes color midway. Logically, this color change can only be perceived after the second dot is presented, implying that later events influence how we perceive earlier ones. Such postdictive effects suggest that conscious perception is not continuous but is preceded by a period of unconscious processing: consciousness is temporally discrete (Herzog et al., 2016, 2020). The discrete nature of consciousness provides a unique opportunity to study the neural correlates of both conscious and unconscious processing, as well as the transitions between the two, using high-temporal resolution imaging techniques like electroencephalography (EEG).

A prime tool for studying these processes is the Sequential Metacontrast (SQM) paradigm (Figures 1A and 1B). In this paradigm, a sequence of vertical lines is presented, creating the illusion of two diverging motion streams expanding from a central point (Otto et

al., 2009, 2010). When one of the lines contains a horizontal vernier offset, all the other lines are perceived as having the same offset, even though they are actually straight. When the stream contains two vernier stimuli with opposite offsets, the offsets *mandatorily* integrate: observers are unable to report the individual offsets separately (Drissi-Daoudi et al., 2019). Instead, they perceive only a single offset, in which either the 1st or 2nd vernier slightly dominates (Menétrey et al., 2023). In general, observers cannot identify which specific lines carry offsets (Drissi-Daoudi et al., 2019).

The mandatory integration period spans approximately 330-450 ms, depending on the observer and the condition (Vogelsang et al., 2023). When two offsets are separated by more than 450ms, observers can report the individual offsets separately (Drissi-Daoudi et al., 2019; Vogelsang et al., 2023). Based on these reports, we proposed that the brain integrates events within a relatively long-lasting window of unconscious processing, followed by a discrete conscious percept. The existence of such long-lasting integration windows has been demonstrated not only in visual perception (Scharnowski et al., 2009; Mudrik et al., 2011; Akyürek & Wolff, 2016; Marti & Dehaene, 2017; Sergent, 2018), but also in auditory perception (McWalter & McDermott, 2019) and across different sensory modalities (Fiebelkorn et al., 2010; Stiles et al., 2018; Rimsky-Robert et al., 2019).

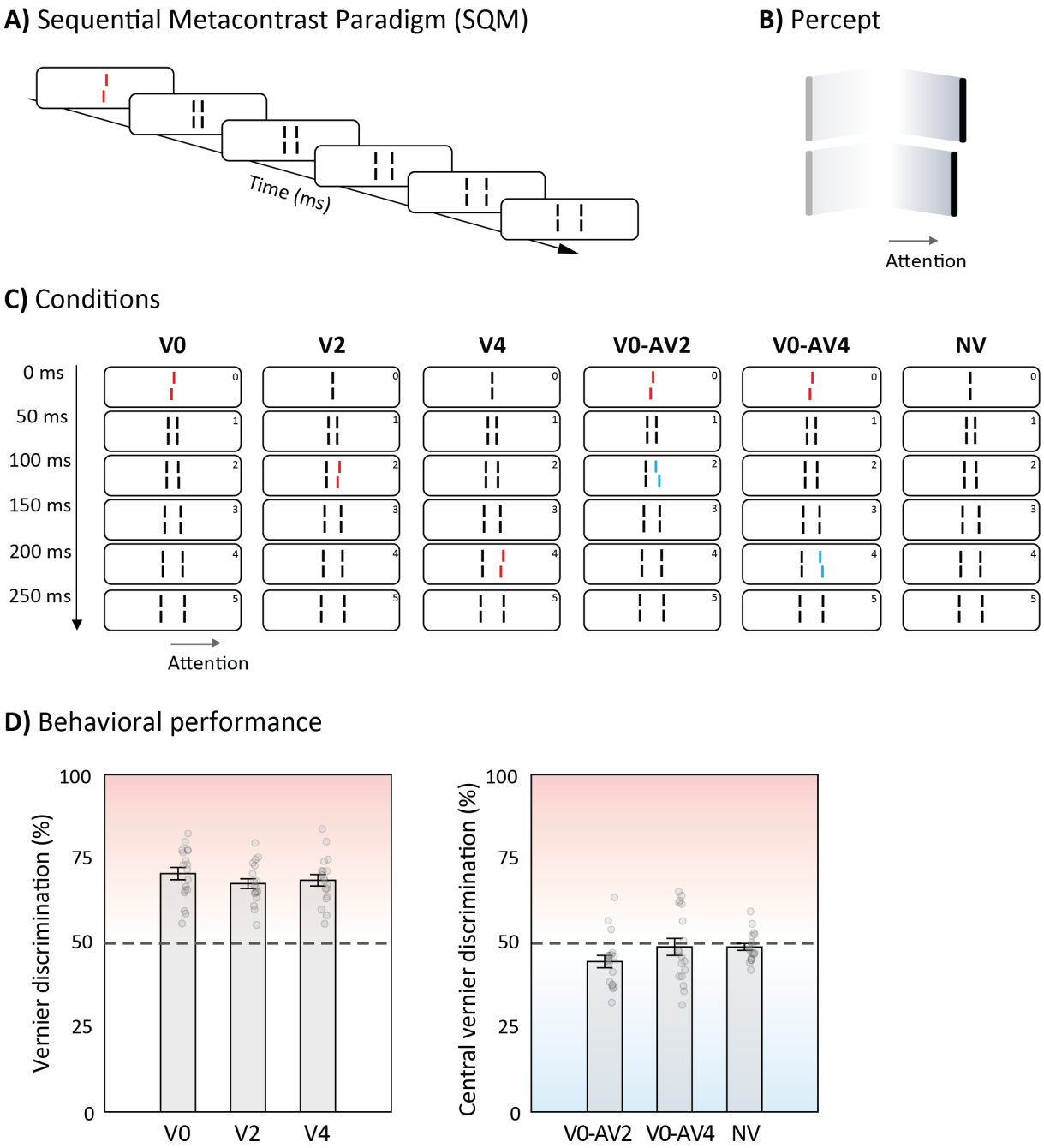

Figure 1. A) The Sequential Metacontrast paradigm (SQM). A central line, here with a left vernier offset, is followed by pairs of flanking lines eliciting a percept of two diverging streams (B). Observers attend to one stream, in which all offsets are integrated. C) In V conditions, only one vernier is presented, either in the central line (V0), in the 2nd (V2), or in the 4th (V4) flanking line. In V-AV conditions, the central line is offset, and one of the flanking is offset in the opposite direction (anti-vernier; V0-AV2 or V0-AV4). In the control condition (NV), only straight lines are shown. The red and blue offset colors in the figure are for illustration purposes only; in the experiment, all lines were the same color. D) Participants attended to the right stream and were asked to report the perceived offset direction (right/left) of the 1st presented vernier offset by pressing hand-held push-buttons. In V conditions, participants could accurately report the offset direction. In V-AV conditions, participants could not perceive the individual vernier offsets, and hence performance is at 50%. This indicates that both vernier offsets contribute equally. When no vernier was presented or perceived, participants were guessing. In NV condition, performance is determined by comparing the response to a randomly chosen offset.

In this study, we used EEG decoding to investigate the neural mechanisms involved in both the unconscious processing of vernier offsets and the subsequent emergence of conscious perception. Our approach was guided by the following rationale: in the SQM, independently of the number and spatiotemporal locations of the verniers in the stream, all offsets are *unconsciously* integrated. Only one offset is consciously perceived, and its size reflects the integration of all unconsciously processed vernier offsets. Consequently, neural activity that encodes information about the number and location of individual vernier offsets are reflecting unconscious processing. By contrast, conscious perception emerges after this unconscious integration. Therefore, neural correlates of conscious perception should reflect the outcome integration—that is, the perceived offset.

Results

Unconscious feature integration within the SQM stream

Participants consistently integrated the vernier offsets with all the lines in the stream, regardless of how many offsets were present, i.e., individual elements in the SQM stream could not be perceived separately (Figure 1A; Drissi-Daoudi et al., 2019; Vogelsang et al., 2023). For example, in the conditions with only a single vernier (V conditions), the offset was perceived as extending across the entire sequence of lines (Otto, 2006; Otto et al., 2010; Figure 1B), and offset discrimination performance was significantly above 50%. This effect was consistent regardless of where the offset appeared in the stream. When the offset occurred in the central line or in the second or fourth flanking lines, the mean accuracy remained high (70% ± 7%). Paired t-tests comparing each of these V conditions with a no vernier (NV) control condition resulted all in significant differences (all $p < .001$, Cohen's $d' > 3.3$; Figure 1D, left panel).

In contrast, when two opposite vernier offsets (a vernier and an anti-vernier) were included in the stream (V-AV condition, Figure 1C), the offsets were mandatorily integrated. Mean accuracy in reporting the 1st offset was 47% ± 9%, comparable to the NV condition (paired t-tests between the V-AV and NV conditions: all $p > .05$; Figure 1D, right panel). Thus, conscious perception does not depend on the location and number of offsets in the stream, as there is no conscious access to individual elements.

Neural representations preserve the chronology of events in the SQM stream

We first aimed to decode neural activity related to the processing of vernier offsets. To this end, we applied Linear Discriminant Analysis (LDA) to EEG activity patterns to decode the presence and location of vernier offsets across the stream.

We ran separate LDA classifiers to discriminate between trials with no offset (NV condition) and trials with a single vernier offset presented at different spatiotemporal locations within the stream (V0: 0 ms, V2: 100 ms, V4: 200 ms, Figure 1C). The classifiers successfully discriminated the presence of a vernier offset in all V conditions (Area Under the Curve, AUC > 0.5, cluster-based permutation test, $p < .05$; Figures 2A and 2B). Crucially, the decoding results revealed systematic delays that corresponded to the actual location of the vernier offset in the stream—decoding was successful at 240 ms for V0 vs. NV, at 330 ms for V2 vs. NV, and at 370 ms for V4 vs. NV (Figure 2B).

Hence, the presence of an offset was decoded approximately 200 ms (170-240 ms) after the vernier's physical onset, despite participants perceiving the offset as present along the entire stream from the beginning (e.g., starting at 0 ms). This result was further supported by a temporal generalization analysis, in which we trained the classifier on data from each time point and tested it across all other time points (see Methods). This analysis revealed similar patterns across conditions, with decoders generalizing only over short time windows, as indicated by higher decoder performance when both training and testing occurred at the same time points (i.e., the diagonal elements of the temporal generalization matrices), and decoding latencies shifted depending on the vernier offset location (Figure 2A).

We then applied cross-condition decoding, training a classifier on discriminating V2 vs. NV or V4 vs. NV and testing it on V0 vs. NV. This revealed shared neural representations of the single vernier across conditions but shifted along the diagonal in the cross-condition temporal generalization matrix (Figure 2C). Specifically, a decoder trained to detect the vernier in the V2 or V4 condition successfully decoded it in V0 (AUC > 0.5, cluster-based permutation test, $p < .05$), but with earlier onsets of approximately 100 and 200 ms, respectively.

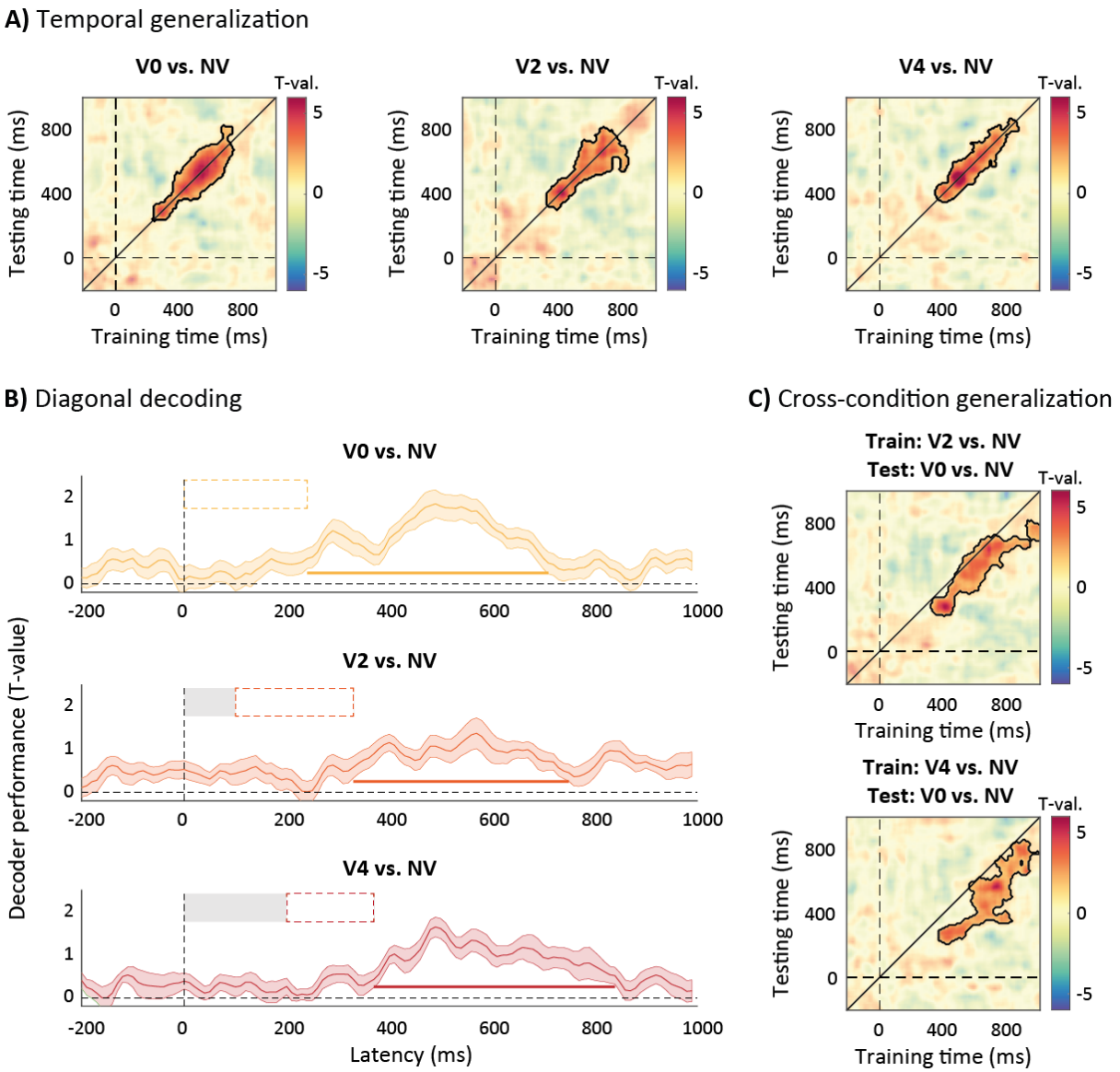

Figure 2. Linear discriminant analysis (LDA) with temporal and cross-condition generalization, decoding conditions with one vernier and no vernier. A) Temporal generalization matrices, obtained by training a classifier on data at every time point and testing it at all other time points, showing that classifiers can successfully discriminate between the conditions (V0, V2, and V4 vs. NV). Significant clusters are highlighted (AUC above 0.5, cluster-based permutation test, $p < .05$). B) Diagonal elements of the temporal generalization matrices, representing decoding results when training and testing at the same time point (group average AUC and 95% CI). Significant time windows are highlighted by the horizontal lines at the bottom. Temporal delays in the decoding results, relative to the actual onset of the vernier in the stream, are indicated by the dashed rectangles. C) Cross-condition generalization matrices demonstrate that classifiers trained with V2 or V4 vs. NV successfully discriminate V0 vs. NV but with earlier onsets corresponding to the effective stimulus delay between V0 and V2 (i.e., 100 ms later) and V4 (i.e., 200 ms later). Significant clusters are highlighted (AUC above 0.5, cluster-based permutation test, $p < .05$).

Decoding the single vernier vs. no vernier conditions was significant in windows ranging from 240 to 710 ms in V0 vs. NV, 330 to 750 ms in V2 vs. NV, and 370 to 840 ms in V4 vs. NV). In these time windows, we found two distinct EEG activation patterns—i.e.,

topographies of EEG activity associated with the decoder results (see Methods and Figure 3A). These scalp patterns and their transitions were consistent across participants (Figure 3A, bottom row, Cohen's *d* of the scalp activation patterns at the group level).

The 1st topography displayed stronger activation over occipital electrodes, with increasing duration as the vernier offset occurred later in the stream (Figure 3B). The 2nd topography, which showed increased activation over parietal electrode sites, had a shorter duration when the vernier offset occurred later (Figure 3B). The time course of these topographies, estimated by back-projecting activation patterns onto the original EEG time series, revealed a clear transition between the two patterns, with evident temporal shifts across conditions (i.e., the transition occurred around 360 ms in V0 vs. NV, 460 ms in V2 vs. NV, and 570 ms in V4 vs. NV; Figure 3C).

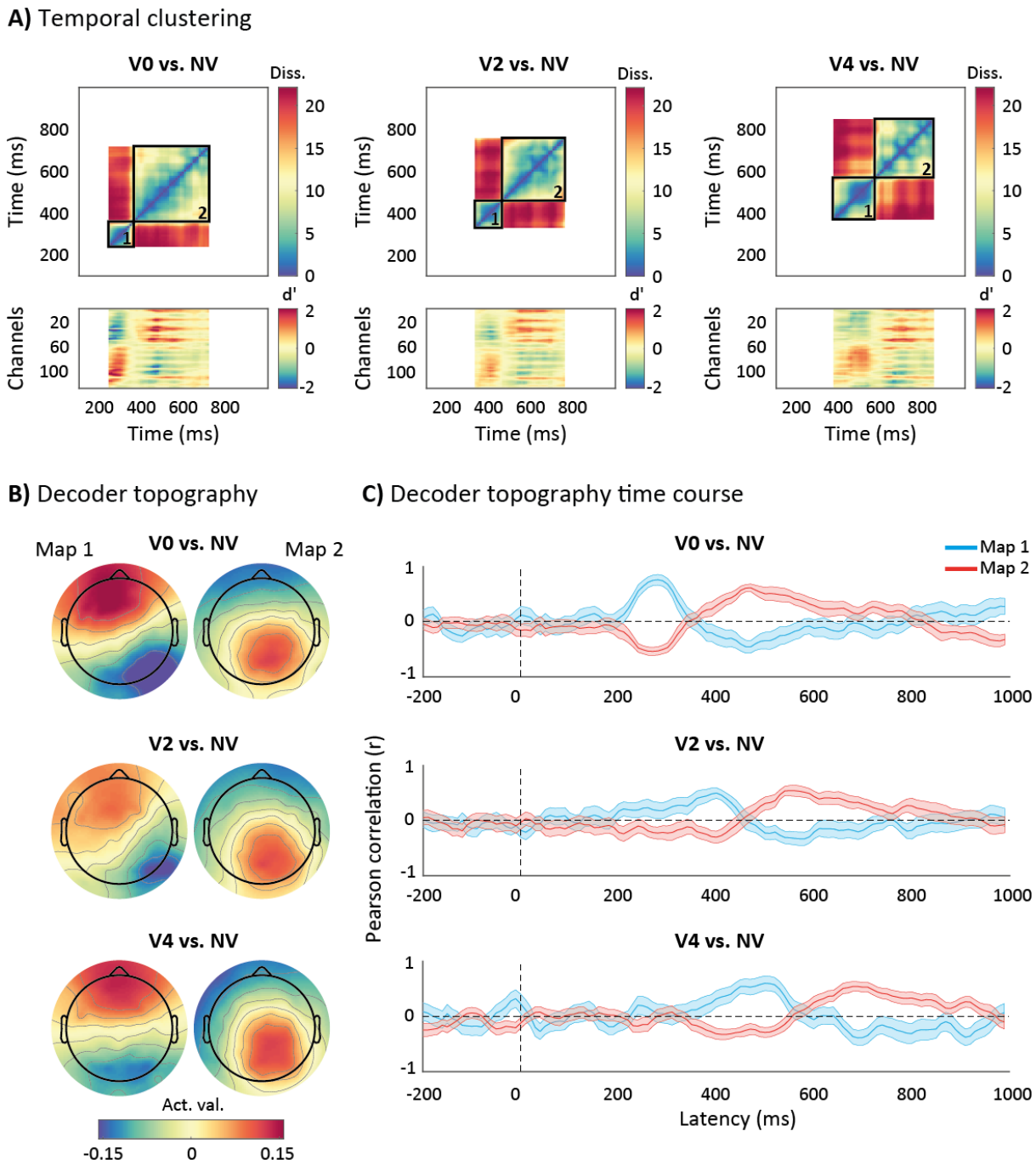

Figure 3. EEG activation patterns contributing to decoding conditions with one vernier and no vernier. A) Analysis of dissimilarity matrices between the EEG activation patterns extracted from significant time points (diagonal elements of the temporal generalization matrices for V0, V2, or V4 vs. NV; see Figure 2B) reveals a clear transition between two main activation patterns (outlined by black squares) for each decoding analysis (upper row). These activations patterns were consistently expressed across participants, as indicated by the large effect sizes (Cohen's *d*) for the difference between each activation pattern and zero, calculated for each electrode and time point (bottom row). B) Decoder topographies, averaged across participants, are derived from the two main activations patterns identified with the analysis of dissimilarity matrices. Each decoding analysis shows similar topographical maps but with variations in their transition dynamics. C) Temporal correlations between the two identified topographies and the back-projected time course of EEG activation patterns for each decoding analysis. Blue and red lines represent the 1st and 2nd maps, respectively. Shaded areas indicate SEM.

Neural correlates of unconscious processing

Up to this point, we have focused on conditions featuring a single vernier, where the vernier is consciously perceived throughout the entire stream. Even though the location of the vernier was not consciously perceived, it could still be decoded via two distinct EEG topographies. Next, we explored conditions involving two opposite vernier offsets, separated by varying intervals (V0-AV2: 50 ms, V0-AV4: 150 ms; Figure 1C), using LDA to distinguish these conditions from a condition featuring only straight lines (NV).

In the V-AV conditions, behavioral performance was around 50%, indicating mandatory integration of the two opposite offsets (Figure 1D). If the two topographies found when decoding the V conditions from the NV condition reflected only the neural correlates of conscious perception, then we would expect no significant decoding for V-AV trials compared to NV trials. However, if one or both topographies are associated with unconscious processing, i.e., before the offsets integrate, we would expect significant decoding.

Consistent with the latter hypothesis, the decoder successfully discriminated V0-AV2 or V0-AV4 trials from NV trials (AUC > 0.5, cluster-based permutation test, $p < .05$; Figure 4A). In both analyses, the significant decoding windows (170-1000 ms) exhibited the same sequence of EEG activation patterns, with topographies (Figure 4C) closely resembling those observed in the V0 vs. NV decoding analysis (Figure 3B). Similarly, the significant decoding onsets and the transition dynamics around 370 ms (Figures 4A and 4D, see also Supplementary Figure S1) closely mirrored those found in V0 vs. NV conditions (Figures 2B, 3A and 3C for comparison). Thus, EEG activation patterns distinguished the presence of two offsets from no offsets, even though the individual offsets were integrated and not perceived separately.

Furthermore, we showed with cross-condition decoding that a decoder trained to detect the vernier in the V0 condition (vs. NV) still successfully decoded, with similar onset and temporal dynamics, V0-AV2 or V0-AV4 conditions from NV condition (AUC > 0.5, cluster-based permutation test, $p < .05$, Figure 4B), confirming a shared neural representations of a single vernier even in conditions with two opposite vernier offsets.

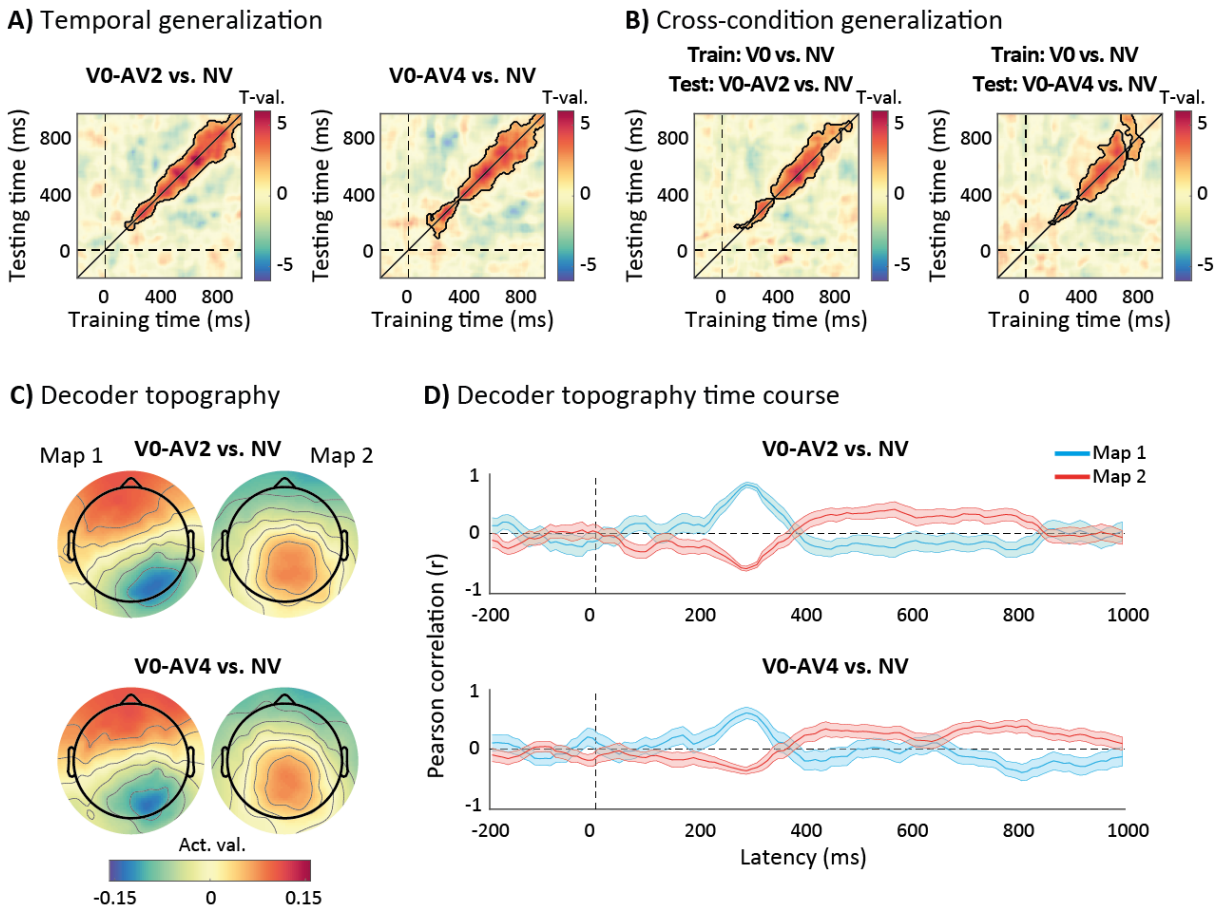

Figure 4. Linear discriminant analysis (LDA) with temporal and cross-condition generalization, decoding conditions with two opposite verniers and no vernier. A) Temporal generalization matrices showing that classifiers successfully discriminate the conditions (V0-AV2 or V0-AV4 vs. NV). Significant clusters are highlighted (AUC above 0.5, cluster-based permutation test, $p < .05$). B) Cross-condition generalization matrices demonstrate that classifiers trained with V0 vs. NV successfully discriminate V0-AV2 or V0-AV4 vs. NV with similar onset. Significant clusters are highlighted (AUC above 0.5, cluster-based permutation test, $p < .05$). C) Decoder topographies, averaged across participants, are derived from the two main activation patterns identified with the analysis of dissimilarity matrices (shown in Supplementary Figure S1). Each decoding analysis shows similar topographical maps and transition dynamics. D) Temporal correlation between the two identified topographies and the back-projected time course of EEG activation patterns for each decoding analysis. Blue and red lines represent the 1st and 2nd maps, respectively. Shaded areas indicate SEM.

Importantly, however, we also found that the two V-AV conditions, where the 2nd offset occurred at different times (V0-AV2 vs. V0-AV4), could be decoded from V0 trials, where only a single vernier was shown and consciously perceived (AUC > 0.5, cluster-based permutation test, $p < .05$; Figure 5A and Supplementary Figure S2). This indicates that neural representations of the 2nd vernier offset were detectable from EEG patterns, even though this offset was not consciously perceived. The significant decoding windows (from 300 ms for V0-AV2 vs. V0, and from 340 ms for V0-AV4 vs. V0) were compatible with the latencies observed when decoding conditions with a single vernier presented later in the stream (V2 or V4 vs NV, Figure 2B), supporting the idea that neural representations of the 2nd vernier remained present.

Moreover, the two V-AV conditions, despite yielding identical conscious percepts, were reliably discriminated from each other (AUC > 0.5, cluster-based permutation test, $p < .05$; Figure 5A and Supplementary Figure S2). That is, EEG activation patterns contained information about the 2nd vernier, which was completely inaccessible to conscious report but decodable starting from 420 ms. Together, these results demonstrate the involvement of one EEG topography (Figure 5B), temporally aligned with the latency of the 2nd vernier, which is highly similar to the 1st topography identified when decoding conditions with one or two offsets from trials without any offset (Figures 3B and 4C).

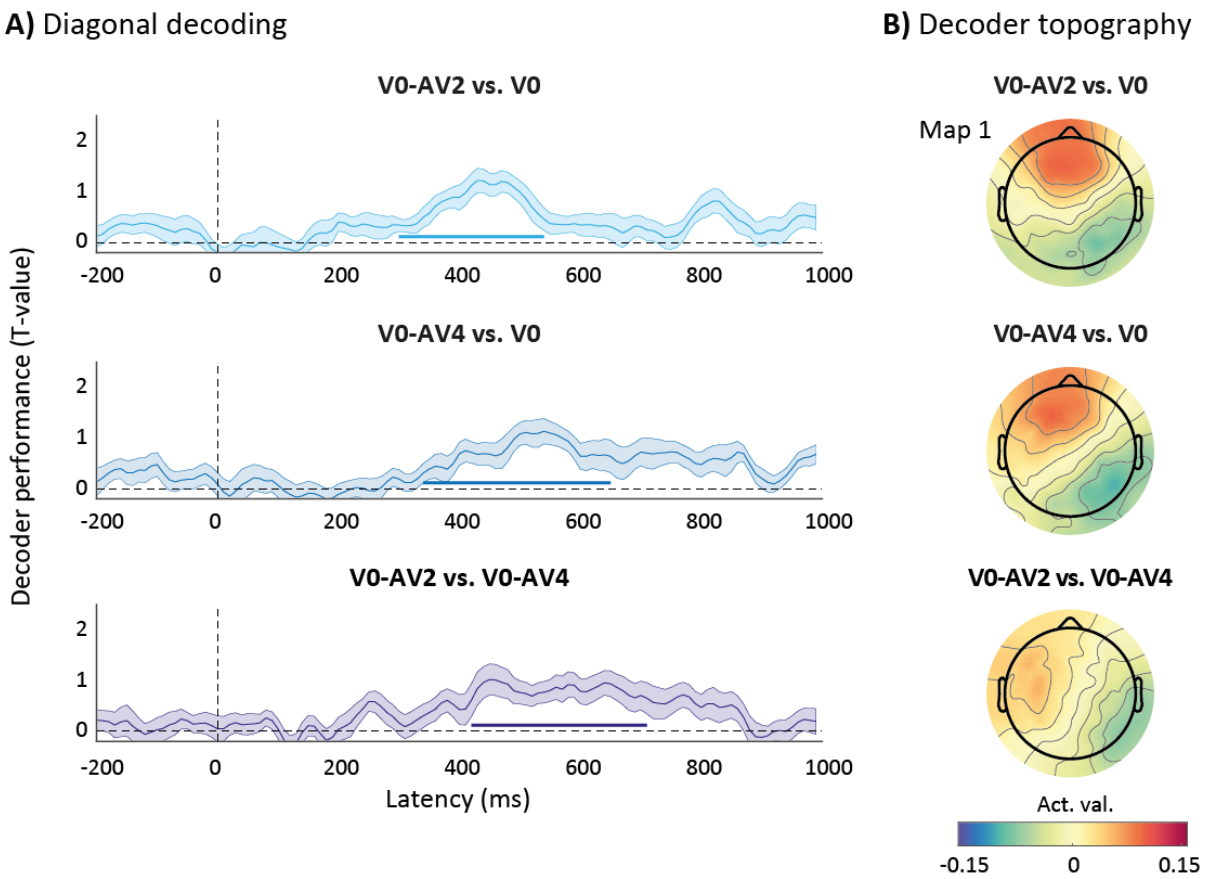

Figure 5. Linear discriminant analysis (LDA) with temporal generalization, decoding conditions with one and two verniers, as well as between the two different conditions with two verniers. A) Diagonal elements of the temporal generalization matrices (shown in Supplementary Figure S2), representing decoding results when training and testing at the same time point (group average AUC and 95% CI). Significant time windows are highlighted by the horizontal lines at the bottom, showing that classifiers successfully discriminate the conditions (V0-AV2 or V0-AV4 vs. V0, and V0-AV2 vs. V0-AV4; AUC above 0.5, cluster-based permutation test, $p < .05$). B) The decoder topographies, averaged across participants, are derived from the averaged activation pattern over the entire significant window of each decoding analysis (see Supplementary Figure S2 for additional evidence that only one activation pattern drives the decoder topography).

Based on these findings, we interpret the 1st topography as the neural correlate of unconscious processing of the vernier stimuli, occurring before the emergence of a conscious

percept. Conversely, the presence of the 2nd topography with a centro-parietal pattern when discriminating V-AV from NV trials (Figure 4C) suggests a 2nd stage in which the integrated percept becomes available to consciousness. As previously suggested (Menétrey et al., 2023), one of the two vernier offsets might dominate the integrated percept in the V-AV condition. Thus, despite chance-level performance, percepts in the V-AV conditions differ from those in the NV condition (i.e., a straight line moving from the center to the periphery). The latencies and sequence of topographies when decoding two opposite verniers from none, which are similar to those observed in the condition with a single vernier presented in the central line (V0; Figure 3B), support this non-uniform integration in V-AV, likely leading to the conscious perception of a smaller integrated vernier in the stream (see also Supplementary Figure S3 for additional cross-condition generalization evidence between V and V-AV conditions, as a function of whether the 1st or 2nd vernier dominated the reported percept).

Neural correlates of conscious perception

To directly assess the involvement of the 2nd topography in conscious perception, we applied LDA to decode correct vs. incorrect reports of the offset direction in the conditions featuring only a single vernier (V conditions). As shown in Figure 6, the classifiers successfully decoded behavioral performance in all single-vernier conditions (Figure 6A; AUC > 0.5, cluster-based permutation test, $p < .05$). However, significant decoding emerged at later latencies—480 ms for V0, 460 ms for V2, and 570 ms for V4—compared to the earlier latencies observed when decoding V or V-AV conditions against the NV condition.

The decoding of the correctly reported direction was characterized by the contribution of a single EEG activation pattern, which perfectly aligned with the 2nd topography identified in previous analyses (Figures 3B and 4C). This finding suggests that the later centro-parietal topography represents the neural correlate of the emergence of a consciously integrated percept, one that becomes available for report. The delayed decoding of correct vs. incorrect responses, compared to the earlier decoding of vernier presence, indicates that this 2nd topography is specifically linked to conscious awareness of the vernier offset, rather than its initial unconscious processing.

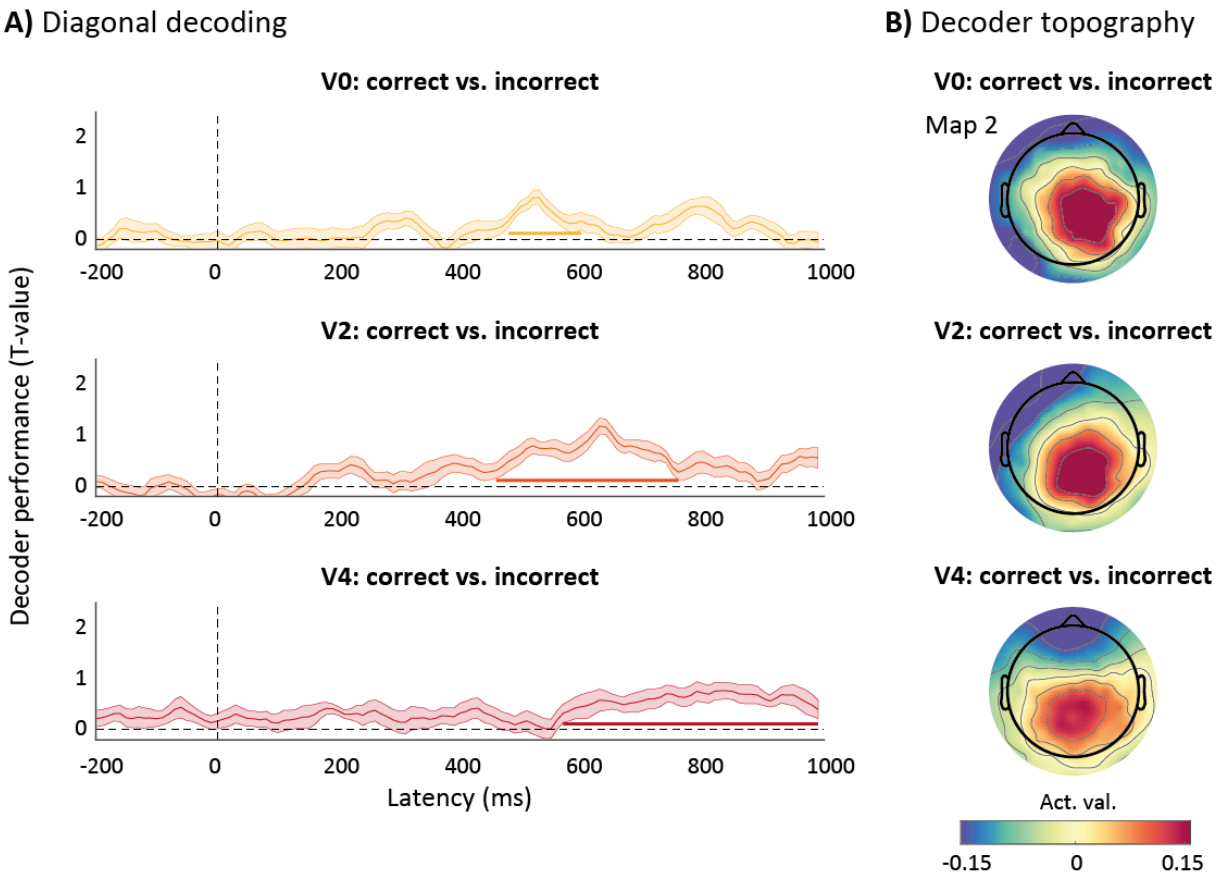

Figure 6. Linear discriminant analysis (LDA) with temporal generalization, decoding correct and incorrect reports in conditions with one vernier. A) Diagonal elements of the temporal generalization matrices (shown in Supplementary Figure S2), representing decoding results when training and testing at the same time point (group average AUC and 95% CI). Significant time windows are highlighted by the horizontal lines at the bottom, showing that classifiers successfully discriminate correct from incorrect offset reports in all V conditions (V0, V2 or V4; AUC above 0.5, cluster-based permutation test, $p < .05$). B) The decoder topographies, averaged across participants, are derived from the averaged activation pattern over the entire significant window of each decoding analysis (see Supplementary Figure S2 for additional evidence that only one activation pattern drives the decoder topography).

Discussion

Previous studies have proposed that conscious perception is preceded by a period of unconscious processing (Herzog et al., 2016, 2020). This is evident in the SQM, where a sequence of lines and offsets is mandatorily and unconsciously integrated for up to 450 milliseconds before a conscious percept emerges (Drissi-Daoudi et al., 2019; Vogelsang et al., 2023). Here, we used time-resolved decoding analysis to investigate the EEG correlates of both unconscious and conscious processing within the SQM paradigm.

Even though the consciously perceived vernier offset does not depend on the number and the specific spatiotemporal location of the verniers within the stream, we can still decode the presence of each vernier from EEG activity patterns time-locked to its actual onset, starting from approximately 200 ms after (Figure 2). The latency of these patterns reflects neural encoding processes that remains inaccessible to conscious awareness and contrasts with the unified percept of a single (moving) offset. This interpretation is further supported by our finding that individual vernier onsets remain decodable even in conditions containing two opposite verniers—where the offsets are obligatorily integrated (Figure 4). Thus, even when individual vernier offsets cannot be consciously perceived, their presence can still be inferred from EEG.

Early decoding was driven predominantly by occipital activity (see Figures 3 and 4). The corresponding topography is consistent with findings from previous studies on the unconscious accumulation and integration of visual information (Fahrenfort et al., 2017; Menétrey et al., 2023) and aligns with the N170/VAN ERP component, which is associated with preconscious processes that engage attention for conscious perception (Koivisto & Revonsuo, 2010; Harris et al., 2013; Cohen et al., 2023). This 1st topography exhibited right-lateralization (ipsilateral to the stimulus). The origin of this lateralization remains unclear, but one possibility is that the right hemisphere dominates processing of motion-related signals from both visual hemifields (Chiappini et al., 2022; Pitcher, 2022), or that it is more generally specialized for visuo-spatial processing (Corballis, 2003).

The same topography was also observed when discriminating between conditions that resulted in a similar integrated conscious percept (i.e., a vernier offset moving along the entire stream) but involving different sequences of unconsciously processed events (i.e., one or two verniers; see Figure 5). Since these conditions differ in the location or even the number of physical offsets, this suggests that this topography reflects differences in the sequence of

unconsciously processed events, supporting its role as a neural correlate of unconscious processing.

Following the occipital topography, we found another distinct centro-parietal topography (see Figures 3 and 4). This 2nd topography contributed to the decoding of conditions where one or more verniers were compared to the condition with no vernier, but it was not observed when discriminating between conditions presenting one or two verniers. This suggests that the later topography is involved in the conscious perception of the integrated offset, independently whether it results from a single vernier or the integration of two. In line with this, the same centro-parietal topography was found when decoding correct vs. incorrect behavioral reports of the offset in conditions with a single vernier (see Figure 6). This late topography emerged after 450 ms and persisted for several hundred milliseconds, resembling the P300 ERP component which is often linked to conscious access (Sergent et al., 2005; Polich, 2007; Rutiku et al., 2015; Silverstein et al., 2015) and thought to signal the availability of information for conscious report (Baars, 2002). Supporting this interpretation, similar topographies have also been associated with consciousness in attentional blink and masking paradigms (Weaver et al., 2019; Noorman et al., 2024).

While the P300 component is compatible with late-access models that associate conscious awareness with higher-order neural processes (Dehaene & Changeux, 2011; Railo et al., 2011; Naccache, 2018; Derda et al., 2019; Ye et al., 2019), it is important to note that observers in our experiment were always required to report the vernier offset. As a result, the signals we are decoding may also reflect post-perceptual processes such as decision-making. In fact, components that are attributed to consciousness, such as the P300, are absent in no-report paradigms (Pitts et al., 2014; Schlossmacher et al., 2020; Cohen et al., 2020; Sergent et al., 2021).

Still, we propose that the transition from the 1st to the 2nd topography reflects a shift from unconscious to conscious processing. This interpretation is supported by the close temporal alignment between the transition and the window of unconscious integration previously estimated through behavioral measures (~330 and 450 ms; Drissi-Daoudi et al., 2019; Vogelsang et al., 2023). The average reaction times were around 900 ms and were not modulated by neither the number nor the locations of verniers in the stream, suggesting that the emergence of the second topography occurred well before the execution of the behavioral response. Thus, we interpret this second topography as related to the period where perceptual information becomes available for report (see also Sergent et al., 2021).

One might argue that the prolonged unconscious stage observed here is specific to the extended motion sequence used in the SQM. However, long-lasting unconscious processing windows have also been reported in other paradigms (Sergent et al., 2013; Akyürek & Wolff, 2016; Thibault et al., 2016; Xia et al., 2016; Sun et al., 2017), suggesting that such extended integration is not specific to the SQM. Importantly, prolonged integration has also been demonstrated with static, briefly presented stimuli. For example, in a paradigm where a 30 ms vernier is followed by a 30 ms anti-vernier, participants perceive a single vernier with one offset. Yet transcranial magnetic stimulation (TMS) can alter this percept up to 360 ms after stimulus onset—well after the stimuli have disappeared from view (Scharnowski et al., 2009). These findings collectively support the idea that unconscious integration can persist well beyond the physical presence of the stimulus.

Our findings further demonstrate that the duration of unconscious and conscious processing and their transition are not fixed but depend on the timing of the 1st vernier offset in the SQM stream. This was most evident when decoding a single vernier against no vernier (Figure 3). The 1st topography lasted slightly longer when the offset was presented later in the stream, while the 2nd topography exhibited a temporal compression, shortening as the offset occurred later (see Figure 3A). It is possible that the occurrence of a vernier offset contributes to the beginning of an unconscious processing window, while the end of the SQM stream may accelerate the collapsing of the sequence into a unified conscious percept. Indeed, offsets presented closer to the end of the entire stream (conditions V2 and V4) might have accelerated the transition from unconscious to conscious processing. Likewise, the decoding delays observed as a function of whether the 1st or 2nd vernier dominated the reported percept (see Supplementary Figure S3) might reflect a temporally extended integration window when the 2nd vernier dominates the final conscious percept. Although the nature of this stimulus-dependent temporal dynamic remains to be fully understood, these results suggest that the temporal structure of neural processing stages is flexible and influenced by subtle details of the stimulus sequence, in contrast to standard ERP analyses that often treat the latencies of processing stages as fixed.

Taken together, our findings support a two-stage model of perception, in which a prolonged period of unconscious processing precedes a discrete conscious percept (Herzog et al., 2016, 2020). During the 1st stage, information is processed with high precision. In this phase, representations of each vernier offset are stored in a high-capacity buffer, where they interact unconsciously (Herzog et al., 2020). At the end of this unconscious processing window, the

buffered information collapses into a conscious percept, reflecting the integrated structure of the entire event. This view is consistent with discrete retentional models of consciousness, in which subjective experience arises as a momentary yet temporally rich event—delayed with respect to stimulus presentation, but containing quantitative information about properties such as stimulus duration, speed, and direction (Herzog et al., 2016).

It is important to distinguish between the timing of neural activity and the timing of conscious perception—a distinction known in philosophy as the "vehicle problem" (Dennett & Kinsbourne, 1992; Herzog et al., 2020; Dainton, 2023). The fact that neural activity is time-locked to a stimulus event (see Figure 2) does not imply that perception occurs at that moment. Just as a neuron that encodes "red" is not itself red, the onset of a neuron's activity does not mark the onset of the corresponding percept (Dennett & Kinsbourne, 1992; White, 2023). This interpretation contrasts with theories that assume a close mapping between the timing of stimuli and the timing of perception—the "brain-time" view (Holcombe, 2014).

In fact, neural activity time-locked to the vernier offset cannot underlie any conscious percept, since, as we argue, it reflects unconscious processing. It is even possible that these signals are discarded during subsequent processing and, for this reason, do not reach awareness. This could explain why observers remain unaware of both the number of verniers and their temporal order.

Similar reasoning applies to the consciously processed signals. We observed a centro-parietal topography lasting approximately 400 ms, which we associate with the emergence of a conscious percept. However, we cannot determine whether this activity pinpoints the precise moment of conscious experience. One possibility, as mentioned above, is that consciousness arises during the transition between neural states—suggesting that conscious perception is discrete and confined to a brief moment in time.

Most theories, with the exception of the global neuronal workspace theory (Dehaene et al., 2006; Dehaene & Changeux, 2011), do not clearly disentangle unconscious from conscious processing stages (for reviews, see Aru et al., 2012; Storm et al., 2017). In this respect, the two-stage nature of conscious perception—unconscious processing followed by a discrete percept—and the underlying neural mechanisms may provide strong constraints for these theories, leading to testable predictions. In particular, our results are of quantitative nature and thus allow precise testing of theories.

In sum, we propose that consciousness is not a continuous stream but is determined by transitions from extended periods of unconscious processing to moments of conscious

perception. This transition between different functional brain states holds critical implications for future research aimed at characterizing the neural correlates of consciousness.

Materials and Methods

Participants

A total of 18 naive, healthy participants (9 females; age range: 18-23 years old) were recruited for the experiment. Participants had normal or corrected to normal vision, as assessed through the Freiburg acuity test (threshold for inclusion: >1; Bach, 1996). All participants signed informed consent before the experiment and received monetary compensation upon its completion. The experiment was conducted in accordance with the local ethics commission and complied with the Declaration of Helsinki (except for pre-registration).

Apparatus

The stimuli were presented on an ASUS VG248QE LCD monitor with a resolution of 1920 x 1080 pixels, a screen size of 24.5 inches, and a refresh rate of 144 Hz. MATLAB R2022b (MathWorks Inc., Natick, MA, USA) along with Psychtoolbox (Brainard, 1997) was used to generate the stimuli. During the experiment, participants were seated at a distance of 1.5 meters from the screen in a dimly lit room. The stimuli appeared as white with a luminance of 100 cd/m², displayed against a uniform black background with a luminance of 1 cd/m².

Stimuli and experimental procedure

We used the sequential metacontrast paradigm (SQM), introduced in Otto et al. (2006), which creates the perception of two motion streams diverging from the center (Figures 1A and 1B). The sequence always began with the presentation of a central vertical line, comprising an upper and a lower segment (the length of each segment is 26.6 arcmin, with a width of 1.2 arcmin) separated by a small vertical gap (2.5 arcmin). Next, pairs of flanking lines appeared progressively further away from the center (horizontal separation between each line is 5 arcmin). The central line and all subsequent pairs of lines were presented for 27.8 ms each, with an interstimulus interval (ISI) of 20.8 ms separating each presentation. The entire stimulus sequence consisted of one central and 5 flanking lines, lasting a total duration of 270.8 ms (Figure 1A).

Participants were instructed to always covertly attend to the right stream. In a randomized order, 6 different conditions were presented (Figure 1C): In the *no vernier* control condition (NV), all lines were straight. In three experimental conditions, one line of the attended stream was offset, with the lower segment shifted either towards the right or the left relative to

the upper segment (referred to as a *vernier offset* or V). In these conditions, the vernier offset was presented either in the 1st central line (V0 condition), in the 2nd flanker line (V2 condition; 100 ms after stimulus onset) or in the 4th flanker line (V4 condition; 200 ms after stimulus onset). In the two last conditions, the central line always had a vernier offset, while another line in the right stream was offset in the opposite direction (referred to as an *anti-vernier* or AV). In these conditions, the opposite vernier was presented either in the 2nd flanker line (V0-AV2 condition) or in the 4th flanker line (V0-AV4 condition).

In all conditions, participants were asked to indicate whether they perceived a left or right offset along the stream (Figure 1B), even when no vernier was presented (usually observers perceive the offset at the last line, even though the line was always straight). Observers were informed that one or two verniers could be presented in the stream and were instructed to report the 1st one in case they perceived both.

Participants completed a total of 12 blocks, with each block consisting of 96 trials (192 trials per condition, 1152 trials in total). Before each trial, a central fixation point was presented for 250 ms, followed by an inter-stimulus interval of 750 ms. After the SQM presentation, participants had 3 seconds to give their response by clicking one of two hand-held buttons. If no response was made within this time, the trial was discarded and repeated at the end of the block. In order to eliminate potential early responses that occurred before the complete presentation of the stimulus sequence, we also excluded trials with reaction times below 300 ms after SQM onset (average number of discarded trials: 8.3 ± 21.2). The inter-trial interval was set at 1 second.

Offset calibration

Before the experiment proper, the offset sizes (i.e., the horizontal displacement between their upper and lower segments) were determined to achieve comparable performance levels across participants. Streams of straight lines with one single vernier were presented, and a parameter estimation by sequential testing (PEST) procedure (Taylor & Creelman, 1967) was used to adaptively determine offset sizes leading to around 70% to 80% performance. This was performed with a vernier offset separately at the three different locations tested in the main experiment: the central line (V0), the 2nd flanker line (V2), or the 4th flanker line (V4).

Behavioral analysis

Performance was determined as the proportion of responses that matched the direction of the 1st presented vernier offset (Figure 1D). We compared performance between the NV condition and each V or V-AV conditions by means of paired t-tests. The NV condition served as a baseline condition; in this condition performance was determined by comparing the response (left or right reported offset) to a randomly chosen notional offset (mean accuracy was 49% ± 4%). All statistical comparisons were Bonferroni-Holm corrected for multiple comparisons (bonf_holm()). When the vernier is presented without an anti-vernier, vernier discrimination should be approximately 75%, in line with the calibration performance. Conversely, when an anti-vernier follows the central vernier, the central vernier discrimination should be around 50%, given the integration of the two verniers. Additionally, we anticipated no performance differences related to the specific locations of the verniers and anti-verniers, as they fell within the same integration window (Drissi-Daoudi et al., 2019). Behavioral performance aligned with this expectation (see Results section).

Across the six tested conditions, average reaction times ranged from 885 ms to 920 ms, with no statistically significant difference between conditions (one-way ANOVA, $F(5, 102) = 0.08$, $p = .99$).

EEG recordings and preprocessing

The EEG data were recorded using a Biosemi Active Two system (Biosemi, Amsterdam, the Netherlands) with a total of 128 Ag–AgCl active electrodes, providing comprehensive scalp coverage. The positioning of the cap was adjusted individually to ensure the Cz electrode was equidistant from the inion and nasion, as well as equidistant from each ear. In addition, the electrooculogram (EOG) was recorded with 4 electrodes positioned 1 cm above and below the right eye and 1 cm lateral to the outer canthi. The recording was referenced to the CMS-DRL ground, maintaining the montage potential close to amplifier zero through a feedback loop. The sampling rate during recording was set at 2048 Hz.

For EEG preprocessing, EEGLAB was utilized (version v2021.1; Delorme et al., 2011; Delorme & Makeig, 2004). The EEG data were first downsampled to 250 Hz. To remove linear trends, detrending was applied (de Cheveigné & Arzounian, 2018), followed by a lowpass filter with a cutoff frequency of 40 Hz. The EEG data were then epoched from -1 s to 1.5 s relative to the onset of the SQM. To ensure data quality, a visual inspection was conducted to identify and exclude epochs (pre-selected with *pop_jointprob* function) or channels with significant

noise or artifacts. Then, an ICA decomposition (*pop_runica* function with Picard algorithm; Ablin et al., 2017a, 2017b) was performed, with a temporary interpolation of the removed channels to maintain a consistent 128-channel configuration across all participants. The ICA decomposition also included "fake" vertical and horizontal EOG recordings, computed from the 4 EOG channels (differences between the channels located above and below the right eye, and between the channels located on the lateral side of each eye). The visually identified independent components associated with eye or muscular artifacts (pre-selected with *pop_icflag* function) were subsequently removed. Lastly, a final interpolation of the removed channels was conducted, along with an average reference including only the EEG channels.

In total, 6.8% of the electrodes were interpolated, while 3.2% of the epochs and 9.1% of the independent components were removed during the preprocessing procedure.

EEG analysis

We aimed to investigate whether brain activity reflects unconscious or conscious processing by decoding differences in EEG dynamics in two configurations of the SQM: 1) when only a single vernier is presented at different locations within the stream (V conditions), with all these conditions resulting in the same percept (i.e., one perceived vernier); and 2) when two opposing verniers are presented (V-AV conditions), yet there is no conscious access to the individual offsets as they integrate.

EEG decoding

Linear discriminant analysis (LDA) with temporal or cross-condition generalization was used to investigate neural representations related to different SQM conditions or percepts. We implemented LDA with custom-made functions written in MATLAB, based on the recommended settings for EEG data (Subasi & Ismail Gursoy, 2010; Grootswagers et al., 2017). For each participant, LDA with temporal generalization was conducted with a leave-one-pseudo-trial-out cross-validation routine (500 iterations). In each iteration, 80% of the trials were sampled and combined into pseudo-trials (average of 20 trials) for the two classes, i.e., the SQM conditions, that were decoded. The mean of the training set was removed to both testing and training sets, and classifier weights were estimated using a regularized covariance (Ledoit & Wolf, 2004; Haufe et al., 2014; Kayser et al., 2016). The classifier weights, obtained from the training set for each time point, were applied to predict the classes in the EEG data of the testing set. Performance was evaluated using the area under the curve (AUC). This process

556 was repeated for each time point (cross-temporal decoding, i.e., each classifier is tested on all
557 time points), ranging from −200 to 1000 ms, with a sliding window of 7 samples corresponding
558 to a resolution of 70 ms (Grootswagers et al., 2017). LDA with cross-condition generalization
559 was performed similarly and with identical parameters, except that the classes used in the
560 training sets differed from those used in the testing sets. For all decoding analyses, EEG data
561 were resampled at 100Hz and z-scored.

562 We started by examining V conditions, where the presentation of a single vernier in the
563 stream results in a clear perception of an offset. We used LDA with temporal generalization to
564 discriminate between trials from the control condition (NV) and trials from conditions
565 presenting one single vernier (V0, V2, or V4), irrespective of the behavioral responses (i.e.,
566 correct or incorrect report of the vernier offset). The classifiers successfully decoded the
567 presence of information regarding the vernier, indicative of either unconscious or conscious
568 processing (Figures 2A and 2B). We also showed some cross-condition generalization between
569 V conditions. Using classifiers trained with V2 or V4 vs. NV conditions, we decoded V0 vs.
570 NV conditions (Figure 2C).

571 Second, we explored the neural representations in the V-AV conditions, where the two
572 opposite verniers integrate with each other. LDA with temporal generalization was used to
573 classify between trials from the NV condition and one of the two conditions presenting two
574 opposite verniers (V0-AV2 or V0-AV4), irrespective of the behavioral responses (i.e., correct
575 or incorrect report of the 1st vernier offset). If V-AV and NV conditions cannot be discriminated,
576 it might suggest that significant decoding observed with V conditions reflects only neural
577 correlates of a clearly visible vernier offset. In this scenario, the two opposite verniers in the V-
578 AV conditions would cancel each other out, resulting in the percept of a straight line, akin to
579 the NV condition. However, this does not appear to be the case as the decoder successfully
580 discriminated between these conditions (Figure 4A; see also Figure 4B and Supplementary
581 Figure S3 for cross-condition generalization between V and V-AV conditions), indicating
582 instead that one of the two offsets still dominates the integrated percept (for similar evidence,
583 see Menétrey et al., 2023). Despite a conscious percept of an offset in all conditions with one
584 or two opposite verniers, we were nevertheless able to decode between V0 and V0-AV2 or V0-
585 AV4 conditions, as well as between the two V-AV conditions, demonstrating that unconscious
586 processing also contributes to this significant decoding (Figure 5A, see also Supplementary
587 Figure S2).

Lastly, we conducted an LDA analysis with temporal generalization to decode between correct and incorrect reports of the offset within each condition presenting one vernier (V0, V2, and V4; Figure 6A, see also Supplementary Figure S2). This analysis aimed to specifically identify neural correlates that reflect conscious perception. All parameters remained consistent with those listed above, except for the averaging of trials for pseudo-trials, which was adjusted to 4 due to the reduced number of available trials, especially the incorrect trials (comprising only ~30% of the total for each condition).

Statistical evaluation of decoding analyses

For all decoding analyses, either with temporal or cross-condition generalization, the statistical evaluation of the 2D matrices of cross-temporal decoding results (subjects x time x time) employed cluster-based permutation approaches and surrogate analysis, following established methodologies (Nichols & Holmes, 2002; Maris & Oostenveld, 2007; Kayser et al., 2016). Clusters were defined as consecutive time points where the decoding successfully exceeded chance levels (chance = 0.5, paired t-test with $\alpha = 0.05$). The cumulative t-values within each cluster were then compared to the maximum sum derived from surrogate clusters (permutations = 10'000). Time points were considered statistically significant if the probability in the surrogate data was <0.05 for the corresponding clusters.

EEG activation patterns

We estimated activation patterns from the LDA classifiers using the regression-based approach (eq. [8] in Haufe et al., 2014). Briefly, this method applies an ordinary least squares regression to derive a pattern that, when multiplied by the discriminant signal obtained via LDA, best approximates the original EEG data used as input to the decoder (electrode x time points x pseudotrials). This approach yields a 'forward model' that allows for neurophysiologically interpretable patterns, addressing the known issue of non-interpretable decoder weights (Haufe et al., 2014; Grootswagers et al., 2017).

We assessed the temporal dynamics of the activation patterns in the context of each decoding analysis (V0, V2, or V4 vs. NV, Figure 2; V0-AV2 or V0-AV4 vs. NV, Figure 4; V0-AV2 or V0-AV4 vs. V0, V0-AV2 vs. V0-AV4, Figure 5; correct vs. incorrect reports in V0, V2, and V4, Figure 6). For each subject, we extracted the activation patterns over the significant time points.

Across the five first decoding contrasts (i.e., all V vs. NV and all V-AV vs. NV conditions; see Figures 2 and 4), we computed time-by-time dissimilarity matrices based on the spatial topographies of decoder activation in order to characterize the temporal structure of EEG activation patterns. First, we averaged activation maps across participants and z-scored the resulting maps across electrodes at each time point to control for overall amplitude differences. We then calculated pairwise dissimilarities between all time points within the significant decoding window using the Euclidean distance—a standard measure of topographic dissimilarity that quantifies how different two z-scored maps are by summing the squared differences across electrodes.

This procedure yielded a symmetric dissimilarity matrix that reflects the similarity structure of spatial patterns over time. To identify periods during which activation patterns remained relatively stable (i.e., dominated by similar topographies), we transformed this dissimilarity matrix into a graph representation, where each node corresponded to a time point and edges were defined between pairs of time points with dissimilarity values below the median of the entire matrix. This thresholding ensured that only relatively similar patterns were considered connected in the graph.

We then applied the Louvain community detection algorithm (Blondel et al., 2008; Rubinov & Sporns, 2010), a widely used method for detecting modular structure in networks, to this graph. In this context, the algorithm grouped together contiguous time points that shared similar activation topographies, thereby identifying clusters of temporally stable EEG patterns. This data-driven clustering allowed us to define distinct temporal clusters characterized by dominant topographic maps (Figures 3A and Supplementary Figure S1), which were used in subsequent analyses.

Topographies of the main activation patterns were then generated by averaging over temporal windows corresponding to the identified clusters (Figures 3B and 4C), revealing two highly consistent spatial topographies. To examine their temporal characteristics and contributions to the overall dynamics, we correlated these spatial patterns with the temporal evolution of EEG activation (back-projected time courses; Figures 3C and 4D). Notably, while the topographies derived from dissimilarity matrices were based on group-averaged data, the back-projection plots demonstrate the consistency of these maps and their temporal dynamics across individuals.

To further assess the reliability of the distinct maps across participants, we estimated Cohen's *d* for the difference between each activation pattern and zero at the level of individual

electrodes and time points (Figures 3A and Supplementary Figure S1). The presence of large effect sizes, both in the positive and negative directions, indicated that the observed topographic patterns were robust and consistently expressed across participants.

For the additional decoding contrasts (i.e., V0 vs. V-AV conditions, V0-AV2 vs. V0-AV4 and correct vs. incorrect reports in V conditions; see Figures 5 and 6), topographies of the main activation patterns were generated by averaging over the entire significant decoding window (Figures 5B and 6B). In addition, we averaged the two maps identified across all decoding results between NV vs. V or V-AV conditions (Figures 3B and 4C) to define two 'prototypical' activation patterns associated with the two distinct processing stages (see Supplementary Figure S2). We then fitted these prototypes to the individual activation patterns from the additional decoding analyses using separate linear models to assess their relative contributions. This analysis confirmed that each decoding result was dominated by a single topography (see Supplementary Figure S2).

Acknowledgments

We sincerely thank Marc Repnow for his excellent technical support.

References

Ablin, P., Cardoso, J.-F., & Gramfort, A. (2017a). *Faster ICA under orthogonal constraint*. https://doi.org/10.48550/ARXIV.1711.10873

Ablin, P., Cardoso, J.-F., & Gramfort, A. (2017b). *Faster independent component analysis by preconditioning with Hessian approximations*. https://doi.org/10.48550/ARXIV.1706.08171

Akyürek, E. G., & Wolff, M. J. (2016). Extended temporal integration in rapid serial visual presentation: Attentional control at Lag 1 and beyond. *Acta Psychologica*, *168*, 50–64. https://doi.org/10.1016/j.actpsy.2016.04.009

Aru, J., Bachmann, T., Singer, W., & Melloni, L. (2012). Distilling the neural correlates of consciousness. *Neuroscience & Biobehavioral Reviews*, *36*(2), 737–746. https://doi.org/10.1016/j.neubiorev.2011.12.003

Baars, B. J. (2002). The conscious access hypothesis: Origins and recent evidence. *Trends in Cognitive Sciences*, *6*(1), 47–52. https://doi.org/10.1016/S1364-6613(00)01819-2

Bach, M. (1996). The Freiburg Visual Acuity Test—Automatic Measurement of Visual Acuity: *Optometry and Vision Science*, *73*(1), 49–53. https://doi.org/10.1097/00006324-199601000-00008

Blondel, V. D., Guillaume, J.-L., Lambiotte, R., & Lefebvre, E. (2008). Fast unfolding of communities in large networks. *Journal of Statistical Mechanics: Theory and Experiment*, *2008*(10), P10008. https://doi.org/10.1088/1742-5468/2008/10/P10008

Brainard, D. H. (1997). The Psychophysics Toolbox. *Spatial Vision*, *10*(4), 433–436.

Chiappini, E., Sel, A., Hibbard, P. B., Avenanti, A., & Romei, V. (2022). Increasing interhemispheric connectivity between human visual motion areas uncovers asymmetric sensitivity to horizontal motion. *Current Biology*, *32*(18), 4064-4070.e3. https://doi.org/10.1016/j.cub.2022.07.050

Cohen, M. A., Keefe, J., & Brady, T. F. (2023). Perceptual Awareness Occurs Along a Graded Continuum: No Evidence of All-or-None Failures in Continuous Reproduction Tasks. *Psychological Science*, *34*(9), 1033–1047. https://doi.org/10.1177/09567976231186798

Cohen, M. A., Ortego, K., Kyroudis, A., & Pitts, M. (2020). Distinguishing the Neural Correlates of Perceptual Awareness and Postperceptual Processing. *The Journal of Neuroscience*, *40*(25), 4925–4935. https://doi.org/10.1523/JNEUROSCI.0120-20.2020

Corballis, P. M. (2003). Visuospatial processing and the right-hemisphere interpreter. *Brain*

and Cognition, *53*(2), 171–176. https://doi.org/10.1016/S0278-2626(03)00103-9

Dainton, B. (2023). *Temporal Consciousness*. https://plato.stanford.edu/archives/spr2023/entries/consciousness-temporal/

de Cheveigné, A., & Arzounian, D. (2018). Robust detrending, rereferencing, outlier detection, and inpainting for multichannel data. *NeuroImage*, *172*, 903–912. https://doi.org/10.1016/j.neuroimage.2018.01.035

Dehaene, S., & Changeux, J.-P. (2011). Experimental and Theoretical Approaches to Conscious Processing. *Neuron*, *70*(2), 200–227. https://doi.org/10.1016/j.neuron.2011.03.018

Dehaene, S., Changeux, J.-P., Naccache, L., Sackur, J., & Sergent, C. (2006). Conscious, preconscious, and subliminal processing: A testable taxonomy. *Trends in Cognitive Sciences*, *10*(5), 204–211. https://doi.org/10.1016/j.tics.2006.03.007

Delorme, A., & Makeig, S. (2004). EEGLAB: An open source toolbox for analysis of single-trial EEG dynamics including independent component analysis. *Journal of Neuroscience Methods*, *134*(1), 9–21. https://doi.org/10.1016/j.jneumeth.2003.10.009

Delorme, A., Mullen, T., Kothe, C., Akalin Acar, Z., Bigdely-Shamlo, N., Vankov, A., & Makeig, S. (2011). EEGLAB, SIFT, NFT, BCILAB, and ERICA: New Tools for Advanced EEG Processing. *Computational Intelligence and Neuroscience*, *2011*, 1–12. https://doi.org/10.1155/2011/130714

Dennett, D. C., & Kinsbourne, M. (1992). Time and the observer: The where and when of consciousness in the brain. *Behavioral and Brain Sciences*, *15*(2), 183–201. https://doi.org/10.1017/S0140525X00068229

Derda, M., Koculak, M., Windey, B., Gociewicz, K., Wierzchoń, M., Cleeremans, A., & Binder, M. (2019). The role of levels of processing in disentangling the ERP signatures of conscious visual processing. *Consciousness and Cognition*, *73*, 102767. https://doi.org/10.1016/j.concog.2019.102767

Drissi-Daoudi, L., Doerig, A., & Herzog, M. H. (2019). Feature integration within discrete time windows. *Nature Communications*, *10*(1), 4901. https://doi.org/10.1038/s41467-019-12919-7

Fahrenfort, J. J., Van Leeuwen, J., Olivers, C. N. L., & Hogendoorn, H. (2017). Perceptual integration without conscious access. *Proceedings of the National Academy of Sciences*, *114*(14), 3744–3749. https://doi.org/10.1073/pnas.1617268114

Fiebelkorn, I. C., Foxe, J. J., Schwartz, T. H., & Molholm, S. (2010). Staying within the lines: The formation of visuospatial boundaries influences multisensory feature integration.

European Journal of Neuroscience, *31*(10), 1737–1743. https://doi.org/10.1111/j.1460-9568.2010.07196.x

Grootswagers, T., Wardle, S. G., & Carlson, T. A. (2017). Decoding Dynamic Brain Patterns from Evoked Responses: A Tutorial on Multivariate Pattern Analysis Applied to Time Series Neuroimaging Data. *Journal of Cognitive Neuroscience*, *29*(4), 677–697. https://doi.org/10.1162/jocn_a_01068

Harris, J. A., McMahon, A. R., & Woldorff, M. G. (2013). Disruption of Visual Awareness during the Attentional Blink Is Reflected by Selective Disruption of Late-stage Neural Processing. *Journal of Cognitive Neuroscience*, *25*(11), 1863–1874. https://doi.org/10.1162/jocn_a_00443

Haufe, S., Meinecke, F., Görgen, K., Dähne, S., Haynes, J.-D., Blankertz, B., & Bießmann, F. (2014). On the interpretation of weight vectors of linear models in multivariate neuroimaging. *NeuroImage*, *87*, 96–110. https://doi.org/10.1016/j.neuroimage.2013.10.067

Herzog, M. H., Drissi-Daoudi, L., & Doerig, A. (2020). All in Good Time: Long-Lasting Postdictive Effects Reveal Discrete Perception. *Trends in Cognitive Sciences*, *24*(10), 826–837. https://doi.org/10.1016/j.tics.2020.07.001

Herzog, M. H., Kammer, T., & Scharnowski, F. (2016). Time Slices: What Is the Duration of a Percept? *PLOS Biology*, *14*(4), e1002433. https://doi.org/10.1371/journal.pbio.1002433

Holcombe, A. (2014). *The Temporal Organization of Perception* (J. Wagemans, Ed.). Oxford University Press. https://doi.org/10.1093/oxfordhb/9780199686858.013.057

Kayser, S. J., McNair, S. W., & Kayser, C. (2016). Prestimulus influences on auditory perception from sensory representations and decision processes. *Proceedings of the National Academy of Sciences*, *113*(17), 4842–4847. https://doi.org/10.1073/pnas.1524087113

Koivisto, M., & Revonsuo, A. (2010). Event-related brain potential correlates of visual awareness. *Neuroscience & Biobehavioral Reviews*, *34*(6), 922–934. https://doi.org/10.1016/j.neubiorev.2009.12.002

Kolers, P. A., & Von Grünau, M. (1976). Shape and color in apparent motion. *Vision Research*, *16*(4), 329–335. https://doi.org/10.1016/0042-6989(76)90192-9

Ledoit, O., & Wolf, M. (2004). A well-conditioned estimator for large-dimensional covariance matrices. *Journal of Multivariate Analysis*, *88*(2), 365–411.

https://doi.org/10.1016/S0047-259X(03)00096-4

Maris, E., & Oostenveld, R. (2007). Nonparametric statistical testing of EEG- and MEG-data. *Journal of Neuroscience Methods*, *164*(1), 177–190. https://doi.org/10.1016/j.jneumeth.2007.03.024

Marti, S., & Dehaene, S. (2017). Discrete and continuous mechanisms of temporal selection in rapid visual streams. *Nature Communications*, *8*(1), 1955. https://doi.org/10.1038/s41467-017-02079-x

McWalter, R., & McDermott, J. H. (2019). Illusory sound texture reveals multi-second statistical completion in auditory scene analysis. *Nature Communications*, *10*(1), 5096. https://doi.org/10.1038/s41467-019-12893-0

Menétrey, M. Q., Herzog, M. H., & Pascucci, D. (2023). Pre-stimulus alpha activity modulates long-lasting unconscious feature integration. *NeuroImage*, *278*, 120298. https://doi.org/10.1016/j.neuroimage.2023.120298

Mudrik, L., Breska, A., Lamy, D., & Deouell, L. Y. (2011). Integration Without Awareness: Expanding the Limits of Unconscious Processing. *Psychological Science*, *22*(6), 764–770. https://doi.org/10.1177/0956797611408736

Naccache, L. (2018). Why and how access consciousness can account for phenomenal consciousness. *Philosophical Transactions of the Royal Society B: Biological Sciences*, *373*(1755), 20170357. https://doi.org/10.1098/rstb.2017.0357

Nichols, T. E., & Holmes, A. P. (2002). Nonparametric permutation tests for functional neuroimaging: A primer with examples. *Human Brain Mapping*, *15*(1), 1–25. https://doi.org/10.1002/hbm.1058

Noorman, S., Stein, T., Fahrenfort, J. J., & Van Gaal, S. (2024). *Distinct neural mechanisms underlying perceptual and attentional impairments of conscious access*. https://doi.org/10.7554/eLife.97900.1

Otto, T. U. (2006). The flight path of the phoenixVThe visible trace of invisible elements in human vision. *Journal of Vision*, 8.

Otto, T. U., Ögmen, H., & Herzog, M. H. (2009). Feature integration across space, time, and orientation. *Journal of Experimental Psychology: Human Perception and Performance*, *35*(6), 1670–1686. https://doi.org/10.1037/a0015798

Otto, T. U., Ogmen, H., & Herzog, M. H. (2010). Attention and non-retinotopic feature integration. *Journal of Vision*, *10*(12), 8–8. https://doi.org/10.1167/10.12.8

Pitcher, D. (2022). Visual motion: Asymmetrical processing differences between the cerebral

hemispheres. *Current Biology*, *32*(18), R957–R960. https://doi.org/10.1016/j.cub.2022.08.005

Pitts, M. A., Padwal, J., Fennelly, D., Martínez, A., & Hillyard, S. A. (2014). Gamma band activity and the P3 reflect post-perceptual processes, not visual awareness. *NeuroImage*, *101*, 337–350. https://doi.org/10.1016/j.neuroimage.2014.07.024

Polich, J. (2007). Updating P300: An integrative theory of P3a and P3b. *Clinical Neurophysiology*, *118*(10), 2128–2148. https://doi.org/10.1016/j.clinph.2007.04.019

Railo, H., Koivisto, M., & Revonsuo, A. (2011). Tracking the processes behind conscious perception: A review of event-related potential correlates of visual consciousness. *Consciousness and Cognition*, *20*(3), 972–983. https://doi.org/10.1016/j.concog.2011.03.019

Rimsky-Robert, D., Störmer, V., Sackur, J., & Sergent, C. (2019). Retrospective auditory cues can improve detection of near-threshold visual targets. *Scientific Reports*, *9*(1), 18966. https://doi.org/10.1038/s41598-019-55261-0

Rubinov, M., & Sporns, O. (2010). Complex network measures of brain connectivity: Uses and interpretations. *NeuroImage*, *52*(3), 1059–1069. https://doi.org/10.1016/j.neuroimage.2009.10.003

Rutiku, R., Martin, M., Bachmann, T., & Aru, J. (2015). Does the P300 reflect conscious perception or its consequences? *Neuroscience*, *298*, 180–189. https://doi.org/10.1016/j.neuroscience.2015.04.029

Scharnowski, F., Ruter, J., Jolij, J., Hermens, F., Kammer, T., & Herzog, M. H. (2009). Long-lasting modulation of feature integrationby transcranial magnetic stimulation. *Journal of Vision*, *9*(6), 1–1. https://doi.org/10.1167/9.6.1

Schlossmacher, I., Dellert, T., Pitts, M., Bruchmann, M., & Straube, T. (2020). Differential Effects of Awareness and Task Relevance on Early and Late ERPs in a No-Report Visual Oddball Paradigm. *The Journal of Neuroscience*, *40*(14), 2906–2913. https://doi.org/10.1523/JNEUROSCI.2077-19.2020

Sergent, C. (2018). The offline stream of conscious representations. *Philosophical Transactions of the Royal Society B: Biological Sciences*, *373*(1755), 20170349. https://doi.org/10.1098/rstb.2017.0349

Sergent, C., Baillet, S., & Dehaene, S. (2005). Timing of the brain events underlying access to consciousness during the attentional blink. *Nature Neuroscience*, *8*(10), 1391–1400. https://doi.org/10.1038/nn1549

Sergent, C., Corazzol, M., Labouret, G., Stockart, F., Wexler, M., King, J.-R., Meyniel, F., & Pressnitzer, D. (2021). Bifurcation in brain dynamics reveals a signature of conscious processing independent of report. *Nature Communications*, *12*(1), 1149. https://doi.org/10.1038/s41467-021-21393-z

Sergent, C., Wyart, V., Babo-Rebelo, M., Cohen, L., Naccache, L., & Tallon-Baudry, C. (2013). Cueing Attention after the Stimulus Is Gone Can Retrospectively Trigger Conscious Perception. *Current Biology*, *23*(2), 150–155. https://doi.org/10.1016/j.cub.2012.11.047

Silverstein, B. H., Snodgrass, M., Shevrin, H., & Kushwaha, R. (2015). P3b, consciousness, and complex unconscious processing. *Cortex*, *73*, 216–227. https://doi.org/10.1016/j.cortex.2015.09.004

Stiles, N. R. B., Li, M., Levitan, C. A., Kamitani, Y., & Shimojo, S. (2018). What you saw is what you will hear: Two new illusions with audiovisual postdictive effects. *PLOS ONE*, *13*(10), e0204217. https://doi.org/10.1371/journal.pone.0204217

Storm, J. F., Boly, M., Casali, A. G., Massimini, M., Olcese, U., Pennartz, C. M. A., & Wilke, M. (2017). Consciousness Regained: Disentangling Mechanisms, Brain Systems, and Behavioral Responses. *The Journal of Neuroscience*, *37*(45), 10882–10893. https://doi.org/10.1523/JNEUROSCI.1838-17.2017

Subasi, A., & Ismail Gursoy, M. (2010). EEG signal classification using PCA, ICA, LDA and support vector machines. *Expert Systems with Applications*, *37*(12), 8659–8666. https://doi.org/10.1016/j.eswa.2010.06.065

Sun, L., Frank, S. M., Hartstein, K. C., Hassan, W., & Tse, P. U. (2017). Back from the future: Volitional postdiction of perceived apparent motion direction. *Vision Research*, *140*, 133–139. https://doi.org/10.1016/j.visres.2017.09.001

Taylor, M. M., & Creelman, C. D. (1967). PEST: Efficient Estimates on Probability Functions. *The Journal of the Acoustical Society of America*, *41*(4A), 782–787. https://doi.org/10.1121/1.1910407

Thibault, L., van den Berg, R., Cavanagh, P., & Sergent, C. (2016). Retrospective Attention Gates Discrete Conscious Access to Past Sensory Stimuli. *PLOS ONE*, *11*(2), e0148504. https://doi.org/10.1371/journal.pone.0148504

Vogelsang, L., Drissi-Daoudi, L., & Herzog, M. H. (2023). Processing load, and not stimulus evidence, determines the duration of unconscious visual feature integration. *Communications Psychology*, *1*(1), 8. https://doi.org/10.1038/s44271-023-00011-2

Weaver, M. D., Fahrenfort, J. J., Belopolsky, A., & Van Gaal, S. (2019). Independent Neural Activity Patterns for Sensory- and Confidence-Based Information Maintenance during Category-Selective Visual Processing. *Eneuro*, *6*(1), ENEURO.0268-18.2018. https://doi.org/10.1523/ENEURO.0268-18.2018

White, P. A. (2023). Time marking in perception. *Neuroscience & Biobehavioral Reviews*, *146*, 105043. https://doi.org/10.1016/j.neubiorev.2023.105043

Xia, Y., Morimoto, Y., & Noguchi, Y. (2016). Retrospective triggering of conscious perception by an interstimulus interaction. *Journal of Vision*, *16*(7), 3. https://doi.org/10.1167/16.7.3

Ye, M., Lyu, Y., Sclodnick, B., & Sun, H.-J. (2019). The P3 Reflects Awareness and Can Be Modulated by Confidence. *Frontiers in Neuroscience*, *13*, 510. https://doi.org/10.3389/fnins.2019.00510

Data Availability

The data supporting the findings of this study are available on the Open Science Framework (https://osf.io/d83vs/)

Conflict of interest

The authors declare no competing financial interests.

Authors contribution statements

M.Q.M, M.H.H. and D.P. conceived the study; M.Q.M collected the data; M.Q.M and D.P. analyzed the data; M.Q.M, M.H.H. and D.P. interpreted the results; M.Q.M, M.H.H., and D.P. wrote the manuscript.

Supplementary Material

EEG activations patterns contributing to decoding conditions with two opposite verniers

The analysis of dissimilarity matrices between the EEG activation patterns extracted from significant time points during the decoding of the two V-AV conditions (V0-AV2 or V0-AV4) vs. the NV condition (Supplementary Figure S1A, see also Figure 4A and Methods) identified two distinct activation patterns (Supplementary Figure S1B, upper row). These patterns exhibited large effect sizes (Cohen's *d*) across different subsets of electrodes (Supplementary Figure SB, bottom row). As shown and discussed in the main manuscript, the corresponding topographies closely resembled those previously identified in decoding V conditions vs. the NV condition (see Figure 3B and Figure 4C for comparison).

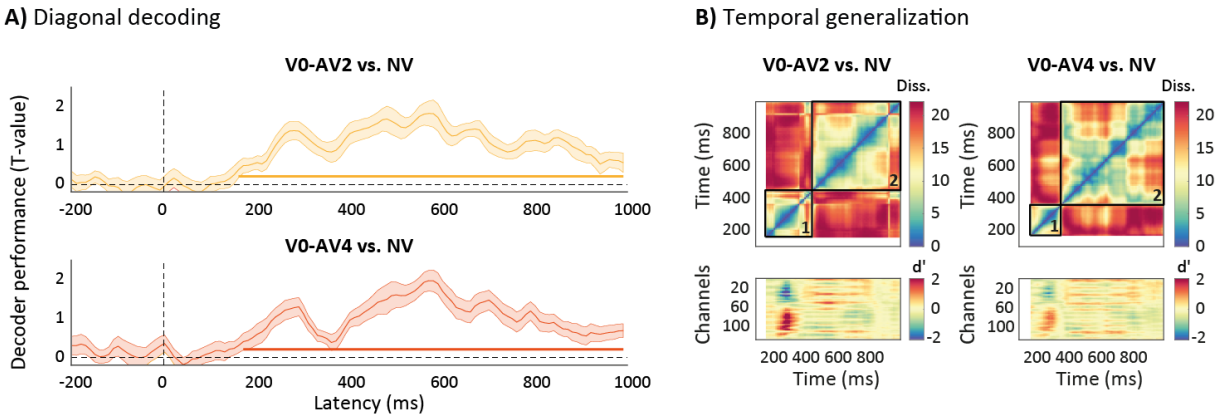

Supplementary Figure S1. A) Diagonal elements of the temporal generalization matrices for V0-AV2 or V0-AV4 vs. NV (see Figure 4A), representing decoding results when training and testing at the same time point (group average AUC and 95% CI). Significant time windows are highlighted by the horizontal lines at the bottom. B) Analysis of dissimilarity matrices between the EEG activation patterns extracted from significant time points reveals a clear transition between two main activation patterns (outlined by black squares) for each decoding analysis (upper row). These activations patterns were consistently expressed across participants, as indicated by the large effect sizes (Cohen's *d*) for the difference between each activation pattern and zero, calculated for each electrode and time point (bottom row).

Correlation with prototypical activation patterns

Two distinct activation patterns, characterized by distinct topographies, were identified in each decoding analysis contrasting the V or V-AV conditions with the NV condition (see Figures 3 and 4). For the remaining decoding analyses—namely, V0 vs. V-AV, V0-AV2 vs. V0-AV4, and correct vs. incorrect responses in V conditions (see Figures 5 and 6)—the topographies of the main activation patterns were obtained by averaging across the entire significant decoding window, corresponding to the diagonal of the temporal generalization matrices (Supplementary Figure S2A).

To evaluate the contribution of the two previously identified topographies to these additional decoding results, we computed two prototypical activation patterns by averaging the corresponding maps across all V or V-AV vs. NV decoding analyses (see Figures 3B and 4C). These prototypes (Supplementary Figure S2B, left) were then correlated with the individual activation patterns from the additional decoding analyses using Pearson correlation, enabling us to quantify their respective contributions to the overall activation patterns. The results confirmed that each decoding contrast was primarily driven by a single topography (Supplementary Figure S2B, right), reflecting either unconscious processing, as in the V0 vs. V-AV and V0-AV2 vs. V0-AV4 contrasts, or conscious perception, as in the contrast between correct and incorrect responses in V conditions.

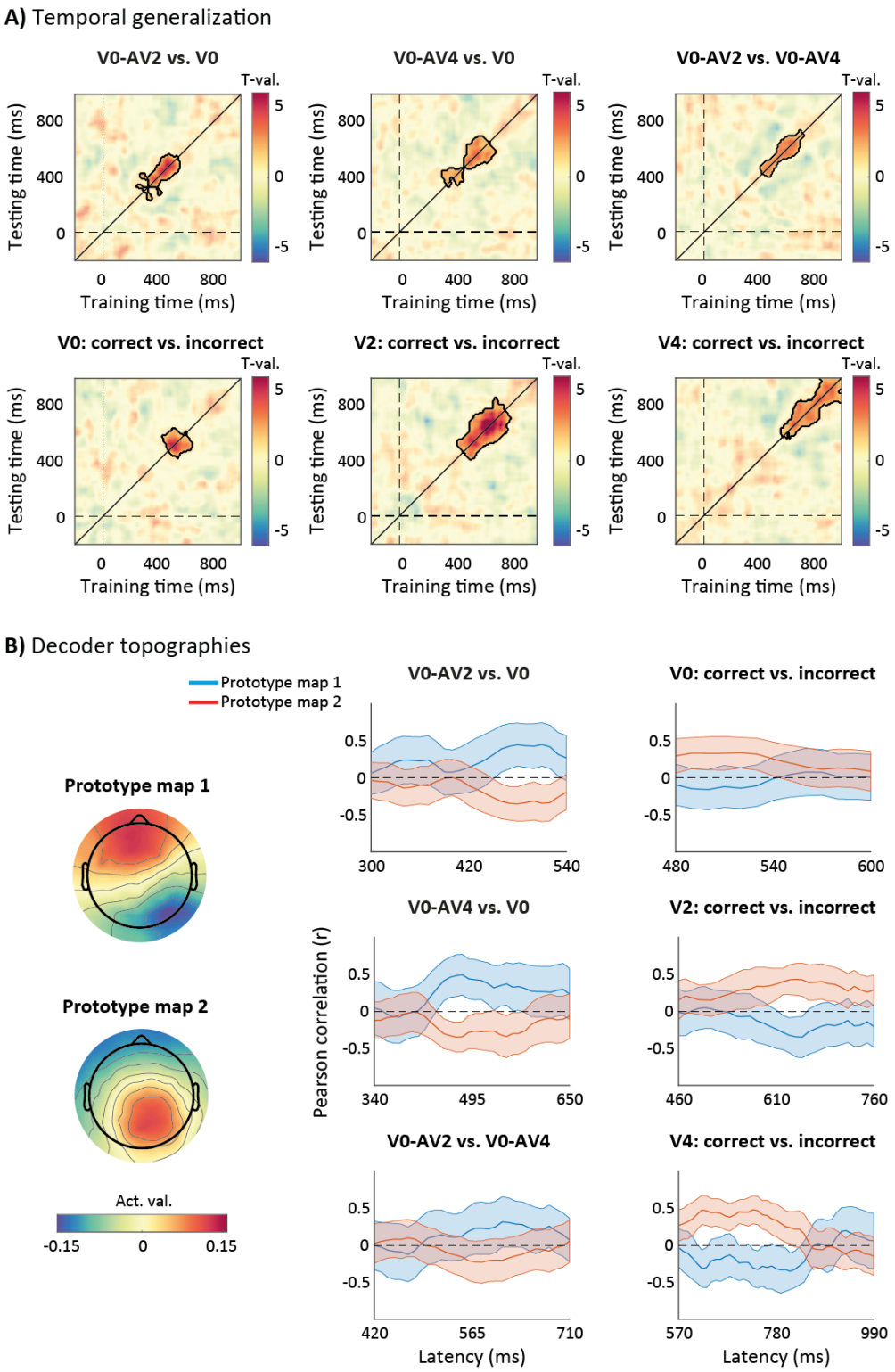

Supplementary Figure S2. A) Temporal generalization matrices showing that classifiers successfully discriminate between conditions with one and two verniers, between two different conditions with two verniers (top row), and between correct and incorrect reports in conditions with one vernier (bottom row). Significant clusters are highlighted (AUC > 0.5; cluster-based permutation test, $p < .05$). B) Prototypical activation patterns (left side), corresponding to the average of the two distinct activation patterns identified via dissimilarity matrix analysis for all V or V-AV vs. NV contrasts (see Figures 3B and 4C), were temporally correlated with the activation patterns found in each significant decoding window (right side). Blue and red lines represent the 1st and 2nd topographies, respectively. Shaded areas indicate the standard error of the mean (SEM).

Cross-condition generalization as a function of the reported vernier (1st or 2nd)

To evaluate the consistency of decoding results, we conducted another set of cross-condition decoding analyses using V-AV conditions. In these analyses, we decoded V-AV conditions from NV conditions using classifiers trained on V conditions (V0, V2 or V4 vs. NV). Only V trials where the reported vernier offset was correct were included to ensure that any decoding results could be linked to conscious processing. Additionally, the classifiers were applied separately to both the V0-AV2 and V0-AV4 conditions, depending on whether the 1st vernier offset (i.e., V0) or the 2nd vernier offset (i.e., V2 or V4) was reported. This approach served two purposes: first, to confirm that a single vernier offset is consistently represented in V-AV conditions, even when the reported percept does not match the central offset (V0); and second, to assess whether the temporal decoding delays previously observed in V conditions (see Figures 2B and 2C) also emerge in V-AV conditions, and whether such delays depend systematically on the spatiotemporal location of the reported vernier.

The cross-condition results successfully decoded V-AV conditions from the NV condition (AUC above 0.5, cluster-based permutation test, $p < .05$; Supplementary Figure S3) in all cases. These results confirm that the EEG patterns related to the V-AV and NV conditions differ (see also Figure 4A) and that a single, integrated vernier is consciously perceived when two opposite verniers are presented (see also Figure 4B). Moreover, they demonstrate that temporal shifts in decoding between training and testing sets, as indicated by significant clusters that are not aligned along the diagonal, directly depend on whether the 1st or 2nd vernier is reported (Supplementary Figure S3). For example, when classifiers trained on V2 or V4 were tested on the V0-AV4 condition, significant decoding clusters appeared primarily below the diagonal; Supplementary Figure S3, lower row), indicating faster decoding in the testing set when the 1st (central) vernier was reported. This effect was more pronounced for classifiers trained on V4 than on V2. Conversely, when the 2nd vernier was reported in the V0-AV4 condition, the significant decoding cluster appeared above the diagonal with classifiers trained on V2, indicating delayed decoding in the testing set. Lastly, classifiers trained on V4 led to a significant decoding cluster aligned along the diagonal, confirming the absence of temporal shift.

These results suggest that although the underlying neural processes in V-AV conditions are similar to those in the V condition (see Figures 2 and 3 for comparison), their temporal dynamics can vary depending on the specific perceptual outcome. Notably, these observed

delays might indicate a temporally extended integration window when the 2nd vernier dominates the final percept.

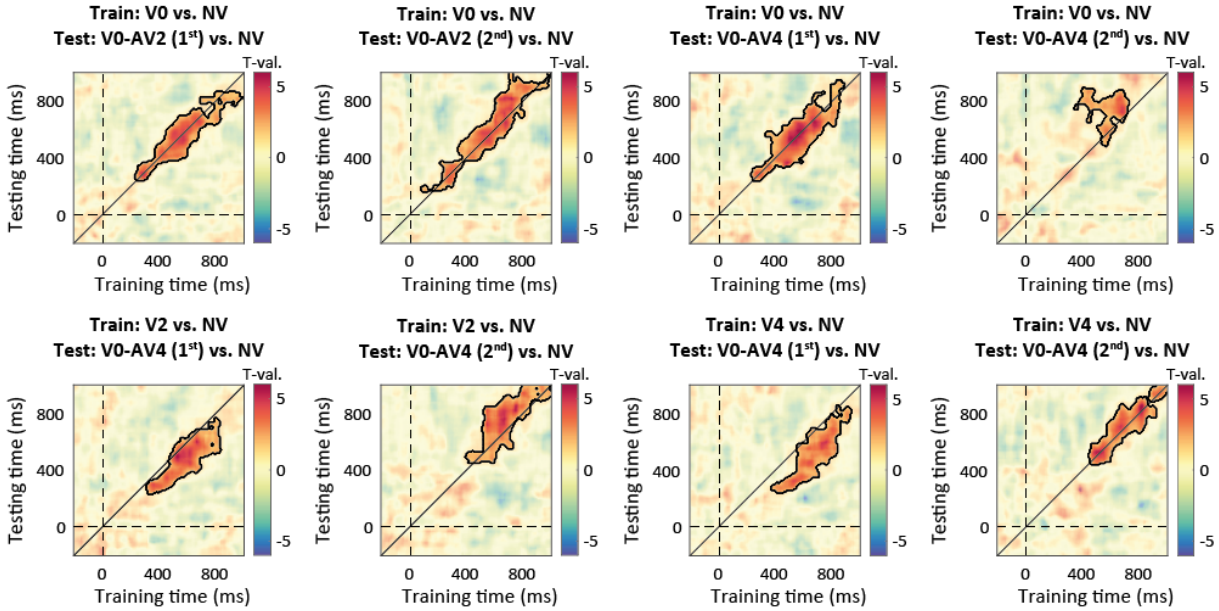

Supplementary Figure S3. Linear discriminant analysis (LDA) with cross-condition generalization. Cross-condition generalization matrices demonstrate that classifiers trained with V conditions (V0, V2 or V4) vs. NV condition successfully discriminate between the two V-AV conditions (V0-AV2 or V0-AV4 vs. NV), regardless of the reported vernier (1st or 2nd). Significant clusters are highlighted (AUC above 0.5, cluster-based permutation test, $p < .05$).